Journal of Power Sources 241 (2013) 404–409

Contents lists available at SciVerse ScienceDirect

Journal of Power Sources

journal homepage: www.elsevier.com/locate/jpowsour

The electrochemical behaviors of Zn–Al–La-hydrotalcite in Zn–Ni secondary cells

Xinming Fan [a], Zhanhong Yang [a,b,*], Xiaoe Xie [a], Wei Long [a], Ruijuan Wang [a], Zhilin Hou [a]

[a] College of Chemistry and Chemical Engineering, Central South University, Changsha 410083, China
[b] Key Laboratory of Resource Chemistry of Nonferrous Metals, Ministry of Education, Central South University, Changsha 410083, China

HIGHLIGHTS

- Zn–Al–La-LDHs were proposed as zinc electrode materials for the first time.
- The electrochemical performances of Zn–Al–La-LDHs were firstly investigated.
- Zn–Al–La-LDHs have superior electrochemical cycle stability.
- The sample of Al/La = 0.8/0.2 (molar ratio) exhibits best electrochemical properties.

ARTICLE INFO

Article history:
Received 17 February 2013
Received in revised form
26 April 2013
Accepted 27 April 2013
Available online 9 May 2013

Keywords:
Zinc–Nickel secondary cells
Zn–Al–La-hydrotalcites
Cyclic voltammograms
Electrochemical performance

ABSTRACT

Zn–Al–La–CO_3 layered double hydroxides (LDHs) are prepared by the constant pH co-precipitation method and proposed as a novel anodic material in Zinc–Nickel secondary cells. The X-ray diffraction (XRD) patterns and scanning electron microscopy (SEM) images reveal that the as-prepared samples are well-crystallized and hexagon layer structure. Electrochemical performances of Zn–Al–La-hydrotalcites with different Zn/Al/La molar ratios are investigated by galvanostatic charge–discharge measurements, cyclic voltammograms (CV) and Tafel polarization curves. In comparison with the Zn–Al-hydrotalcite, Zn–Al–La-hydrotalcites with different Zn/Al/La molar ratios have more stable cycling performance. After 400 cell cycles, Zn–Al–La-LDH with Zn/Al/La = 3:0.8:0.2 retains specific discharge capacity of 297 mAh g^{-1} with a retention rate of 79.0%, which is much superior to that of 205 mAh g^{-1} with a retention rate of 53.5% for the Zn–Al–La-LDH with Zn/Al/La = 3:0.9:0.1 and 241 mAh g^{-1} with a retention rate of 69.0% for the Zn–Al–La-LDH with Zn/Al/La = 3:0.6:0.4. The results demonstrate that the Zn–Al–La-LDH with Zn/Al/La = 3:0.8:0.2 has the best reversible cycling behavior. The CV exhibits well reversibility and the Tafel polarization curves reveal more positive corrosion potential for Zn–Al–La-hydrotalcite.

1. Introduction

Zinc/Nickel (Zn–Ni) alkaline secondary system is a promising candidate for the new generation of green power sources used in electric vehicle (EV) or hybrid electric vehicle (HEV) in recent years. It has attractive advantages of high energy and power densities, high open circuit voltage, excellent low-temperature performance, low cost and environment friendly [1–5]. However, the commercial applications of Zn–Ni alkaline secondary batteries are severely limited by their poor cycling characteristic, which mainly results from the drawbacks of zinc electrode, such as shape change, zinc dendrite formation, surface passivation, zinc self-corrosion and self-discharge [6,7]. These problems derive from a high solubility of the discharge products of zinc electrode in alkaline electrolyte and non-uniform deposition of zinc active material during charging [8,9]. Various attempts, such as the use of additives in either the anode [2,10] or the electrolyte [11,12], the modification of Zn electrode [9] and calcium zincate as the anodic active material [13], have been made to overcome the shape change and dissolution problems of the Zn electrode. Nevertheless, these approaches could not effectively overcome these obstacles. Therefore, we need to find a novel anode material for Zn–Ni secondary batteries which can remarkably increase cell lifetime and improve electrochemical performance.

Layered double hydroxides (LDHs), or hydrotalcite similar to LDHs, with a general formula of $[M_a(II)_{1-x}M_b(III)_x(OH)_2]^{x+}(A^{n-}_{x/n})\cdot MH_2O$ (where M_a and M_b are metal ions), consist of positively charged brucite-like layers, whose net charge is compensated by

* Corresponding author. College of Chemistry and Chemical Engineering, Central South University, Changsha 410083, China. Tel./fax: +86 731 88879616.
E-mail addresses: zhyang@mail.csu.edu.cn, zhongnan320@gmail.com (Z. Yang).

0378-7753/$ – see front matter © 2013 Elsevier B.V. All rights reserved.
http://dx.doi.org/10.1016/j.jpowsour.2013.04.136

easily exchanged anions located in the interlayer (the typical layer structure of LDH shown in Fig. 1), have been widely studied in fields of catalysts [14], drug delivery materials [15], nanofillers [16] and chemically tailored functional materials [17]. In particular, the electrochemistry properties of LDHs as new modified electrodes have been attracted much attention [18–21]. Among LDHs, Zn–Al-LDHs employed as novel anodic material for Zn–Ni secondary battery were investigated by us [22]. In the two-dimensional layered structures, the zinc hydroxide is arranged orderly on a layer and aluminum hydroxide is on the other parallel layer. The aluminum ions are conductive to zinc active material to form crystal nucleus during deposition, so as to deplete overgrowth of zinc grain, such as zinc moss and dendrites [23]. However, Zn–Al-LDHs suffer low conductivity and largely suppress the electron transfer for electrode reaction. Therefore, it is valuable for the modification of Zn–Al-LDHs to enhance its electrochemical properties.

Compounds of lanthanum elements such as lanthanum oxide and lanthanum hydroxide have been used as additives for the zinc electrode [24,25]. In the present work, Zn–Al–La-LDHs have been proposed as zinc electrode materials for the first time and the electrochemical properties were studied in details. For comparison, the electrochemical performance of Zn–Al-LDHs electrode was investigated.

2. Experimental

2.1. The preparation of Zn–Al–La-hydrotalcites

The Zn–Al–La-LDHs were prepared by co-precipitation. An aqueous solution (450 ml) of Zn, Al and La nitrates (with Zn:Al:La molar ratio equal to 3:1:0, 3:0.9:0.1, 3:0.8:0.2 and 3:0.6:0.4) and total metal ion concentration of 1.0 mol dm^{-3} was added with flow rate of 80 ml min^{-1} into batch reactor containing 200 ml of distilled water. The flow rate of simultaneously added alkaline solution of 0.5 mol dm^{-3} Na_2CO_3 and 2 mol dm^{-3} NaOH was controlled to maintain the reaction pH of 10. The co-precipitation was carried out under vigorous stirring at 25 °C. The product was filtered off and a part of filtration cake was placed into 100 ml Teflon lined stainless steel bomb and resuspended in filtrate (mother liquor) to obtain 75 ml of suspension containing about 10 wt% of solid, which was hydrothermally treated at 180 °C for 12 h. After filtration, the product was washed thoroughly with distilled water and dried overnight at 60 °C.

2.2. The characterization of Zn–Al–La-hydrotalcites

Fourier transform infrared (FT-IR) spectroscopy were conducted on a Nicolet Nexus-670 FT-IR spectrometer (as KBr discs, with wave number 400–4000 cm^{-1}, resolution 0.09 cm^{-1}, and the weight of measured sample 2 mg). X-ray diffraction (XRD) was performed on a D500 (Siemens) diffractometer (36 kV, 30 mA) using Cu Kα radiation at a scanning rate of $2\theta = 8^\circ$ min^{-1}. The morphology of as-synthesized Zn–Al–La-LDHs was observed using scanning electron microscope (SEM, JSM-6360LV).

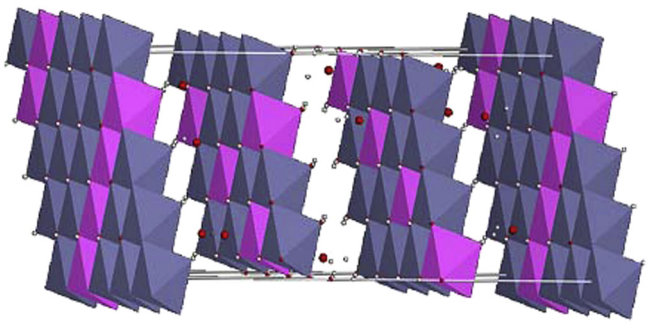

Fig. 1. The typical layer structure of LDH (divalent and trivalent metal cations form lamellar structure, anions located in the interlayer).

2.3. The preparation of Zn–Al–La-hydrotalcites electrodes

The Zn–Al–La-LDHs electrodes were prepared by incorporating slurries containing Zn–Al–La-LDHs, acetylene black and Polytetrafluoroethylene (PTFE, in diluted emulsion) to a copper mesh substrate (1.0 cm × 1.0 cm in size). The weight ratio of Zn–Al–La-LDHs, acetylene black, and PTFE was 80:10:10. The obtained zinc electrodes were dried at 80 °C under vacuum and pressed to a thickness of 0.30 mm. For comparison, Zn–Al-LDH electrodes composed of Zn–Al-LDHs were also fabricated by the same way. A two-electrode cell was assembled for pre-activated testing of cell. A solution of 5.5 mol dm^{-3} KOH, 1.0 mol dm^{-3} NaOH and 0.5 mol dm^{-3} LiOH was used as the electrolyte. The polypropylene micro-porous membrane was used as the separator. The sintered Nickel electrodes were used as positive electrodes. The Zn–Al–La-LDHs electrode and sintered Nickel electrode were assembled into a cell and placed in a single cell container made of Perspex. The capacity of the sintered Nickel electrode was far more than that of the Zn–Al–La-LDHs electrode on the purpose of making full use of Zn–Al–La-LDHs material during cycling. The alkaline Zn–Ni secondary cells were pre-activated at the charging current density of 0.1 C for 10 h, and then discharged at 0.2 C to 1.4 V cut-off for three times at room temperature.

2.4. The measurements of electrochemical properties

The galvanostatic charge–discharge tests were performed on a BTS-5V/10 mA battery-testing instrument (Neware, China) at room temperature. A two-electrode cell was assembled for cyclic testing of cell. Other test conditions are the same as pre-activated step. During the cycling process, the cells were charged at 1 C for 60 min and discharged at 1 C down to 1.4 V cut-off voltages. A three-electrode cell was assembled for cyclic voltammograms (CV) and Tafel polarization, with Hg/HgO electrode served as the reference electrode, pre-activated pasted zinc electrode as the working electrode and the sintered Nickel electrode as counter electrode. The capacity of counter electrode was far higher than that of zinc electrode. The electrolyte was 6 mol dm^{-3} KOH solution. CV test was carried out on an electrochemical workstation (CHI660B) at room temperature at a scanning rate of 5 mV s^{-1} range from −0.95 V to −1.65 V. Tafel polarization curves were also carried out using an electrochemical workstation (CHI660B) at room temperature at a scanning rate of 0.5 mV s^{-1}.

3. Results and discussions

3.1. The FT-IR analysis of Zn–Al–La-hydrotalcites

For the samples of Zn–Al–La-hydrotalcites with different Al/La molar ratio, the FT-IR spectra in Fig. 2 were very similar. The broad peak around 3440 cm^{-1} can be ascribed to the stretching of OH^- groups attached to metal ions. The bending vibration of interlayer water is found at 1650 cm^{-1}. The O–C–O asymmetric stretching vibration appears between 1350 and 1550 cm^{-1}. And a considerably lower shifted absorption peak at 1362 cm^{-1}, as compared with CO_3^{2-} of $CaCO_3$ (1430 cm^{-1}), shows that there was an intercalation between CO_3^{2-} and interlayer H_2O through the strong hydrogen bonding. The lower wave number bands at 400–700 cm^{-1} is due to LDH lattice vibrations (Zn–O, Al–O, La–O, La–O–Zn). The bands at 775 cm^{-1} and 553 cm^{-1} can be assigned to Al–O stretching modes.

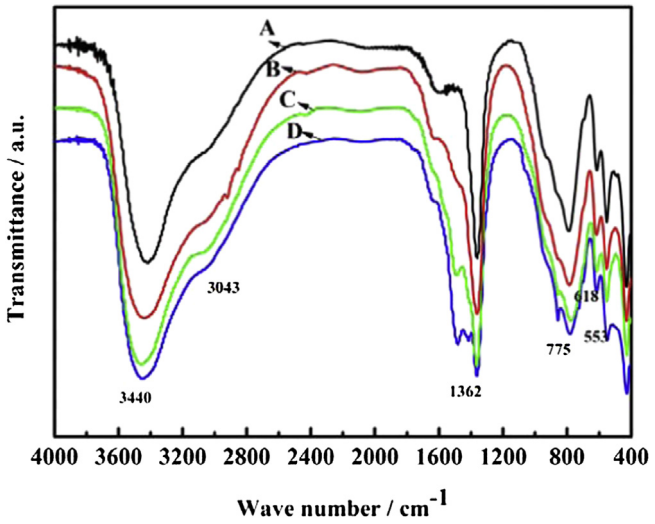

Fig. 2. FT-IR spectra of Zn–Al-hydrotalcite and Zn–Al–La-hydrotalcites with different Zn/Al/La molar ratio A: Zn/Al/ = 3/1, B: Zn/Al/La = 3/0.9/0.1, C: Zn/Al/La = 3/0.8/0.2, D: Zn/Al/La = 3/0.6/0.4.

These Al–O peaks of Zn–Al–La-hydrotalcites are weaker than those of Zn–Al-hydrotalcite, which probably resulted from the partial replacement of La^{3+}. As Aluminum atomic radius (1.82 Å) and lanthanum atomic radius (2.74 Å) are not significant and they are both trivalent ions, partial aluminum atoms in lattice can be replaced by Lanthanum atoms. The molecular structure of Zn–Al-LDH and Zn–Al–La-LDH from different perspectives is represented in Fig. 3. As shown in Fig. 3, aluminum atoms can be replaced by lanthanum atoms, the structure of LDH remains the same. The strong band at 428 cm^{-1} in Fig. 2 belongs to the layered skeleton structure of hydrotalcite. It was basically the same as that of the LDH without La element. Hence, it is safe to conclude that La had been introduced into the lattice of hydrotalcite.

3.2. The XRD and SEM analysis of Zn–Al–La-hydrotalcites

Fig. 4a shows the XRD pattern of as-prepared Zn–Al-LDH and Zn–Al–La-LDHs powder, respectively. As seen in Fig. 4a, the

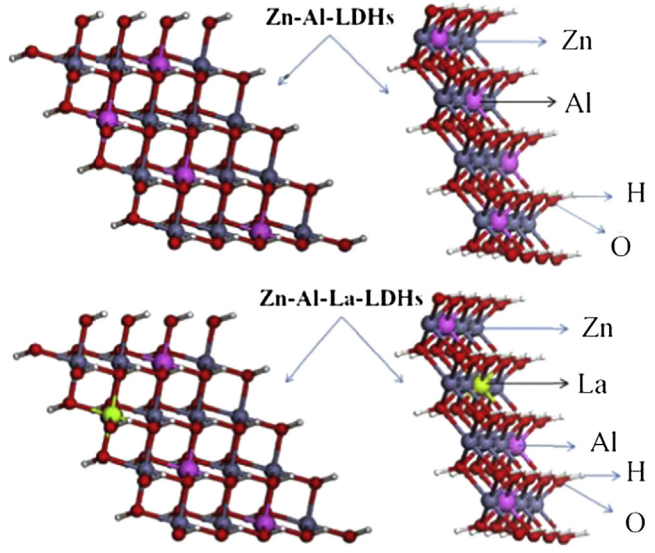

Fig. 3. The molecular structure of Zn–Al-hydrotalcite and Zn–Al–La-hydrotalcites from different perspectives.

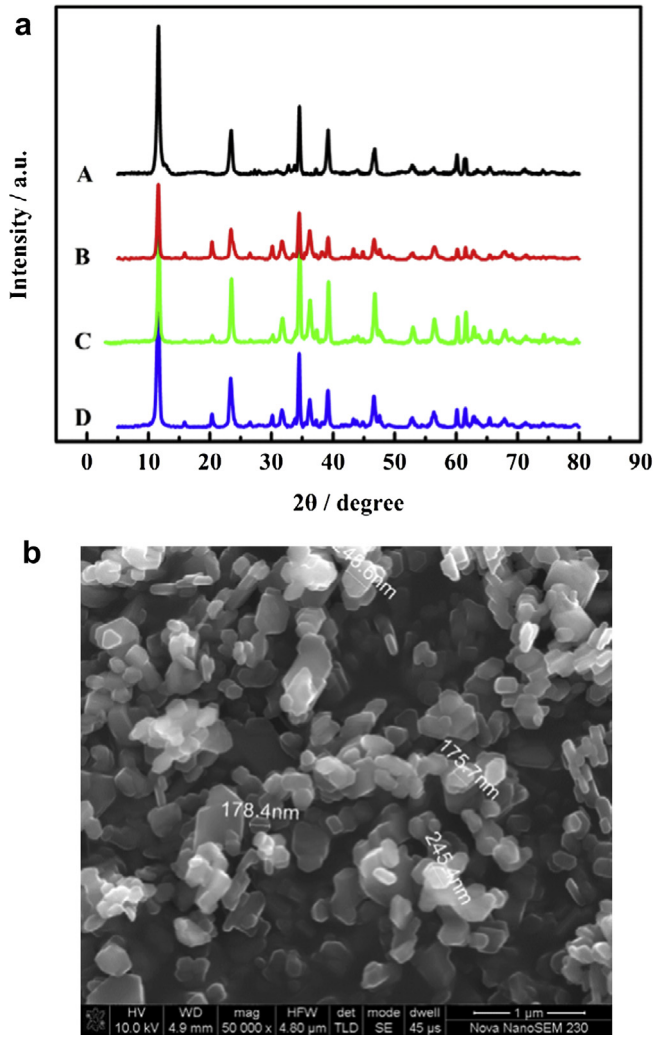

Fig. 4. a) The XRD pattern of as-prepared Zn–Al-hydrotalcite and Zn–Al–La-hydrotalcites with different Zn/Al/La molar ratio A: Zn/Al = 3/1, B: Zn/Al/La = 3/0.9/0.1, C: Zn/Al/La = 3/0.8/0.2, D: Zn/Al/La = 3/0.6/0.4. b) The typical SEM image of Zn–Al–La-hydrotalcite with Zn:Al:La = 3:0.8:0.2.

diffraction peaks (at 2θ = 11.72, 23.56, 34.56, and 61.66) of Zn–Al–La-LDHs are corresponding to the relations of (003), (006), (009) and (110) accordingly, which can also be seen in that of Zn–Al-LDH. The diffraction peaks are sharp, narrow and symmetrical, with a low and stable baseline, indicating that the sample is well-crystallized. The highest diffraction peak appears at 2θ = 11.72°, suggesting the hydrotalcite-like compound Zn–Al–La-LDHs are highly crystallized and has a typical hexagonal crystal structure. Note that the XRD patterns of Zn–Al–La-LDHs with different Zn/Al/La molar ratios are similar. The results indicate that Zn–Al–La-LDHs could be successfully synthesized with different Zn/Al/La molar ratios. According to Fig. 4a, the diffraction peak of curve C is sharper than that of B and D, indicating that the Zn–Al–La-LDH with Zn:Al:La = 3:0.8:0.2 has high crystallinity and integrated crystalline structures.

The typical SEM image of Zn–Al–La-LDH with Zn:Al:La = 3:0.8:0.2 was presented in Fig. 4b. It can be seen that the existing lamellar particles have hexagon layer structure, which is the typical structure of the hydrotalcite-like material [26]. As shown in Fig. 4b, the particle size of Zn–Al–La-LDH is about 175–250 nm.

3.3. The cycle performance analysis of Zn–Al–La-LDHs electrodes

Fig. 5a presents the variation of specific discharge capacity with the number cycles for the Zn–Al-LDH and Zn–Al–La-LDHs with different Al/La molar ratio. As shown in Fig. 5a, it can be found that all electrodes suffer from the low capacity for the first several cycles due to the incomplete activation of the active material in the electrodes. During the subsequent cycles, the active material is gradually activated. Then, the discharge capacity of each electrode recovers. Although the discharge capacity of the Zn–Al-LDH is maximum (388.3 mA h g^{-1}), it declines rapidly after 30 cycles. At the 50th cycle, the discharge capacity decreases to 262.2 mA h g^{-1} with the capacity retention ratio (discharge capacity/the maximum discharge capacity) of 67.5%. For comparison, all Zn–Al–La-LDHs, namely B, C and D show more excellent cycle stability in the 50 times' cycle. The initial discharge capacity of B, C and D is 344.9 mA h g^{-1}, 327.2 mA h g^{-1} and 313.9 mA h g^{-1}, respectively. The results show that the initial discharge capacity decreases with the increase of La content in Zn–Al–La-LDHs. The main reason is that the lanthanum elements have a larger molar mass than aluminum element. Consequently, the content of active components in zinc electrode decreases. In order to further illuminate the effects of different Al/La molar ratio on the electrochemical properties of Zn–Ni secondary cell, cycling performances of Zn–Al–La-LDHs with different Al/La molar ratio are continue to 400 cycles (Fig. 5b). As shown in Fig. 5b, after 400 cycles the Zn–Al–La-LDH with Zn:Al:La = 3:0.8:0.2 retains a specific discharge capacity of 297.0 mA h g^{-1} with a retention rate of 79.0%, which is much superior to that of 205.0 mA h g^{-1} with a retention rate of 53.5% for the Zn–Al–La-LDH with Zn:Al:La = 3:0.9:0.1 and 241.0 mA h g^{-1} with a retention rate of 69.0% for the Zn–Al–La-LDH with Zn:Al:La = 3:0.6:0.4. The above results demonstrate that the Zn–Al–La-LDH with Zn:Al:La = 3:0.8:0.2 shows the best stable cycle performance. The main reason is generally attributed to the rare-earth La elements. During the charge process, bivalent zinc ions are reduced into zinc metal. And a possible reaction can be represented by Equation (1). And Equation (1) consists of Equation (2)–(6).

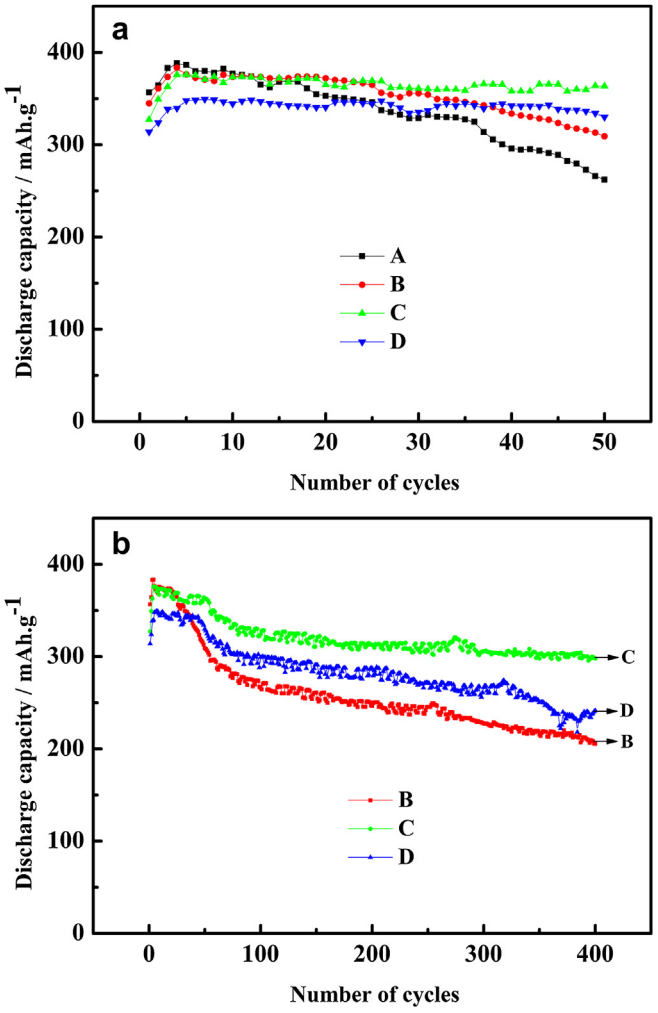

Fig. 5. Electrochemical cycle behavior of Zinc–Nickel secondary cells with Zn–Al-hydrotalcite and different Zn/Al/La molar ratios of Zn–Al–La-hydrotalcites. A: Zn/Al = 3/1, B: Zn/Al/La = 3/0.9/0.1, C: Zn/Al/La = 3/0.8/0.2, D: Zn/Al/La = 3/0.6/0.4.

$$[Zn_{1-x-y}Al_xLa_y(OH)_2]^{(x+y)+}(CO_3)^{2n-}_{(x+y)/2n}\cdot mH_2O + 2(1-x-y)e = (1-x-y)Zn + (x/2)Al_2O_3 + (y/2)La_2O_3 + (2-3x-3y)OH^- + ((x+y)/2n)CO_3^{2n-} + ((3x+3y+2m)/2)H_2O \quad (1)$$

$$[Zn_{1-x-y}Al_xLa_y(OH)_2]^{(x+y)+}(CO_3)^{2n-}_{(x+y)/2n}\cdot mH_2O = (1-x-y)Zn^{2+} + xAl^{3+} + yLa^{3+} + 2OH^- + ((x+y)/2n)CO_3^{2n-}\cdot \quad (2)$$

$$Zn^{2+} + 4OH^- \rightarrow Zn(OH)_4^{2-} \quad (3)$$

$$Zn(OH)_4^{2-} + 2e \rightarrow Zn + 4OH^- \quad (4)$$

$$2Al^{3+} + 6OH^- \rightarrow 2Al(OH)_3 \leftrightarrow Al_2O_3\cdot 3H_2O \quad (5)$$

$$2La^{3+} + 6OH^- \rightarrow 2La(OH)_3 \leftrightarrow La_2O_3\cdot 3H_2O \quad (6)$$

However, Element Al, La exists in the form of oxides [Al_2O_3/$Al(OH)_3$ and La_2O_3/$La(OH)_3$] in the electrode [22,25], respectively. Two factors can contribute to it. Firstly, in theory, for the reduction reaction, the standard electrode potential is more negative, the reaction occurs more difficultly. The hydrated oxide [$Al(OH)_3$ and $La(OH)_3$] cannot be reduced into aluminum and Lanthanum metal at charging process, as the standard electrode potential of $Zn(OH)_4^{2-}$/Zn (−1.199 V) is larger than that of $Al(OH)_3$/Al (−2.31 V) and $La(OH)_3$/La (−2.90 V) in alkaline solution.

$$Zn(OH)_4^{2-} + 2e \leftrightarrow Zn + 4OH^- \quad E\Theta = -1.199\ V \quad (7)$$

$$Al(OH)_3 + 3e \leftrightarrow Al + 3OH^- \quad E\Theta = -2.31\ V \quad (8)$$

$$La(OH)_3 + 3e \leftrightarrow La + 3OH^- \quad E\Theta = -2.90\ V \quad (9)$$

Secondly, according to our previous report, namely Ref. [22], we have tested XRD patterns of Zn–Al-LDH electrode after complete discharge and analysis the phase transformations of the Zn–Al-LDH during the electrode cycling. So it can be seen that Al exist as oxides after discharging. Moreover, The XPS results in Ref. [25] can be seen that La existed in the form of oxides [La_2O_3/$La(OH)_3$] in the electrode.

During the discharge process, except most of Zn metal is oxidized into Zn–Al–La-LDHs, some of Zn metal is oxidized into the byproduct-ZnO, which have been exploited by us [22]. ZnO has dendrite growth in charge–discharge process [27]. La oxide [La_2O_3/$La(OH)_3$] layer is believed to prevent the dissolution of partial discharge products and suppress the dendrite growth [25]. For the Zn–Al–La-LDH with Zn:Al:La = 3:0.9:0.1, the La_2O_3 amount of the

formation is relatively few due to the adding less amount of La, which cannot effectively prevent the dissolution of partial discharge products and suppress the dendrite growth. In particular, as atomic radius of La (2.74 Å) is larger than that of Al (1.82 Å), an excessive La additive leads to disproportionation of Lattice which impacts cycle stability of the Zn–Al–La-LDH with Zn:Al:La = 3:0.6:0.4. Consequently, as a novel anodic material, the Zn–Al–La-LDH with Zn:Al:La = 3:0.8:0.2 shows the most excellent cycling performance among Zn–Al–La-LDHs.

3.4. The properties of galvanostatic charge and discharge

The typical charge–discharge curves of Zn–Ni batteries using the Zn–Al-LDH and Zn–Al–La-LDHs electrodes tested at 25th cycle are displayed in Fig. 6a. The overall electrode reaction can be described as Equations (10) and (11).

Charge process

$$Zn(OH)_4^{2-} + 2e \rightarrow Zn + 4OH^- \quad (10)$$

Discharge process

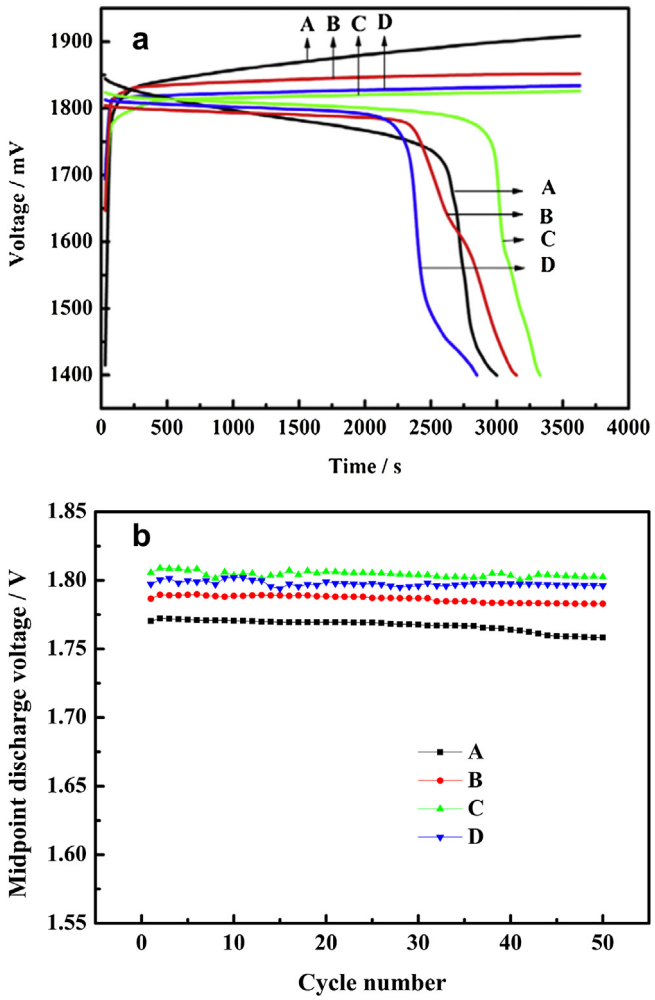

Fig. 6. a) Typical galvanostatic charge–discharge curves of Zinc–Nickel secondary cells with Zn–Al-hydrotalcite and different Zn/Al/La molar ratios of Zn–Al–La-hydrotalcites at the 25th cycle. A: Zn/Al = 3/1, B: Zn/Al/La = 3/0.9/0.1, C: Zn/Al/La = 3/0.8/0.2, D: Zn/Al/La = 3/0.6/0.4. b) Midpoint discharge voltage curves of Zinc–Nickel secondary cells with Zn–Al-hydrotalcite and different Zn/Al/La molar ratios of Zn–Al–La-hydrotalcites A: Zn/Al = 3/1, B: Zn/Al/La = 3/0.9/0.1, C: Zn/Al/La = 3/0.8/0.2, D: Zn/Al/La = 3/0.6/0.4, A: Zn/Al = 3/1, B: Zn/Al/La = 3/0.9/0.1, C: Zn/Al/La = 3/0.8/0.2, D: Zn/Al/La = 3/0.6/0.4.

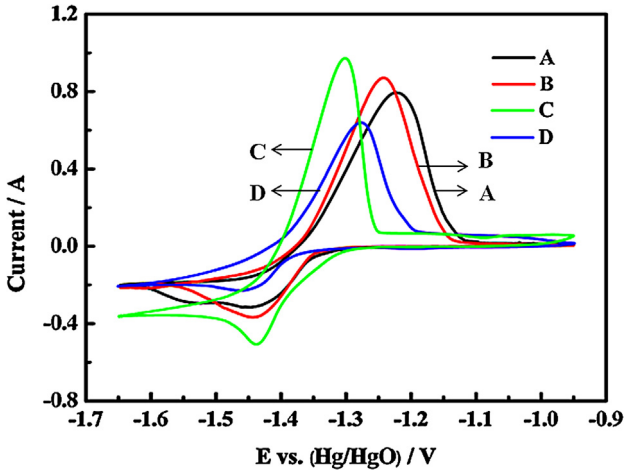

Fig. 7. Cyclic voltammogram for zinc electrodes with Zn–Al-hydrotalcite and different Zn/Al/La molar ratios of Zn–Al–La-hydrotalcites A: Zn/Al = 3/1, B: Zn/Al/La = 3/0.9/0.1, C: Zn/Al/La = 3/0.8/0.2, D: Zn/Al/La = 3/0.6/0.4.

$$Zn + 4OH^- \rightarrow Zn(OH)_4^{2-} + 2e \quad (11)$$

As observed, the cell employed with the Zn–Al–La-LDHs presents a lower charge plateau voltage and higher discharge plateau voltage than that of the Zn–Al-LDH. Especially, the cell employed for the Zn–Al–La-LDH with Zn:Al:La = 3:0.8:0.2 shows lowest charge plateau voltage and highest discharge plateau voltage. The decrease in charge plateau voltage is advantaged to the suppression of H_2 formation and improvement of charge efficiency. Furthermore, higher discharge plateau voltage associates with higher discharge potential and better performance in discharge process. The performance of the Zn–Al–La-LDHs electrodes was further investigated by the midpoint discharge voltage of the battery. The curves of midpoint discharge voltage vs. number of cycles for the Zn–Al-LDH and Zn–Al–La-LDHs electrodes are displayed in Fig. 6b. The average midpoint discharge plateau voltage of Zn–Al–La-LDH with Zn:Al:La = 3:0.8:0.2 was 35 mV higher than that of Zn–Al-LDH, 20 mV higher than Zn–Al–La-LDH with Zn:Al:La = 3:0.9:0.1 and 10 mV higher than Zn–Al–La-LDH with Zn:Al:La = 3:0.6:0.4.

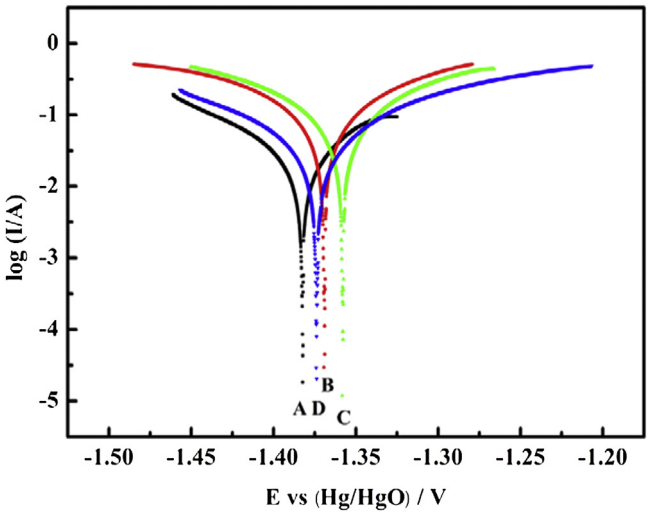

Fig. 8. Tafel polarization curves for zinc electrodes with Zn–Al-hydrotalcite and different Zn/Al/La molar ratios of Zn–Al–La-hydrotalcites A: Zn/Al = 3/1, B: Zn/Al/La = 3/0.9/0.1, C: Zn/Al/La = 3/0.8/0.2, D: Zn/Al/La = 3/0.6/0.4.

Table 1
The data for the Tafel curves for zinc electrodes with Zn–Al-hydrotalcite and different Zn/Al/La molar ratios of Zn–Al–La-hydrotalcites. A: Zn/Al = 3/1, B: Zn/Al/La = 3/0.9/0.1, C: Zn/Al/La = 3/0.8/0.2, D: Zn/Al/La = 3/0.6/0.4.

Sample	E_{corr} (V)	I_{corr} (mA cm^{-2})	I.E.%
A	−1.3823	9.49×10^{-2}	–
B	−1.3694	4.81×10^{-2}	49.3
C	−1.3578	2.26×10^{-2}	76.2
D	−1. 3738	3.48×10^{-2}	63.4

3.5. The results of cyclic voltammograms (CV)

In order to further investigate electrochemical performance of Zn–Al-LDH and Zn–Al–La-LDHs with different Zn/Al/La molar ration, CV studies were carried out and the recorded CV curves are shown in Fig. 7. As shown in Fig. 7, the anodic peaks of zinc electrodes containing the Zn–Al-LDH (code A), Zn–Al–La-LDH with Zn:Al:La = 3:0.9:0.1 (code B), Zn–Al–La-LDH with Zn:Al:La = 3:0.8:0.2 (code C) and Zn–Al–La-LDH with Zn:Al:La = 3:0.6:0.4 (code D) appear at −1.2227 V, −1.2419 V, −1.3015 V and −1.2785 V, respectively. Compared with zinc electrode A, B and D, zinc electrode C shows higher anodic peak current, larger anodic peak area and lower anodic peak potential. The anodic process reflects the discharge process of Zn–Ni secondary battery. The increase in anodic peak area and anodic peak current means that zinc electrode C possesses the higher electrochemical activity, and can deliver more discharge capacity than that of zinc electrode A, B and D, which is consistent with the charge/discharge performance of the zinc electrode C shown in Fig. 5a. The decrease in anodic peak potential shows the discharge process of zinc electrode C can occur in lower potential, so Zn–Ni secondary battery with zinc electrode C delivers higher discharge voltage.

3.6. The Tafel polarization curves of Zn–Al–La-LDHs electrodes

For understanding the changes of corrosion protection properties of Zn–Al–La-hydrotalcites on the performance of zinc electrode, Tafel polarization experiments are carried out. Fig. 8 shows the Tafel curves of zinc electrodes, whose Zn:Al:La (molar ratio) is 3:1:0, 3:0.9:0.1, 3:0.8:0.2 and 3:0.6:0.4 respectively, are coded A, B, C and D electrodes. The electrochemical kinetic parameters derive from these curves are given in Table 1. The kinetic parameters include corrosion potential (E_{corr}), corrosion current density (I_{corr}), and inhibition efficiency (I.E.%). The inhibition efficiency is calculated by Refs. [28–30]:

$$\text{I.E.\%} = \left(I^0_{corr} - I_{corr}\right) \Big/ I^0_{corr} \times 100 \quad (12)$$

where I^0_{corr} and I_{corr} are the corrosion current densities of zinc electrodes without and with La additive, respectively. It is clear from that the curve for Zn–Al–La-LDHs sample is shifted to slightly larger the corrosion potential and significantly lower the corrosion currents compared to Zn–Al-LDH sample. With the increase of La contents, E_{corr} is slightly shifted to positive direction and I_{corr} decreases. Especially, from Table 1 Zn–Al–La-LDH with Zn:Al:La = 3:0.8:0.2 exhibits the most positive steady-state corrosion potential and lowest corrosion current. As a result, inhibition efficiency of Zn–Al–La-LDH with Zn:Al:La = 3:0.8:0.2 is the largest. The high inhibition efficiency of the Zn–Al–La-LDHs electrode is attributed to the La additive with high corrosion resistance and high over-potential of hydrogen evolution [30]. The high over-potential of hydrogen evolution can inhibit hydrogen evolution reaction of Zn–Al–La-LDHs electrode, so that the corrosion of Zn–Al–La-LDHs electrode can be slowed on alkaline solution.

4. Conclusion

Zn–Al–La-hydrotalcites with different Al/La molar ratio have been fabricated by co-precipitation method. The structure and electrochemical performance of Zn–Ni secondary cell with Zn–Al–La-hydrotalcites as the negative electrode is investigated. Zn–Al–La-hydrotalcites are highly crystallized to be the hexagonal crystal structure. Zn–Al–La-hydrotalcites with different Al/La molar ration, especially the sample of Al/La = 0.8/0.2 (molar ratio), employed as negative electrode of Zn–Ni battery exhibits good reversibility, more positive corrosion potential, superior electrochemical cycling stability and more excellent utilization ration compared with the Zn–Al-hydrotalcite electrode. Therefore, Zn–Al–La-hydrotalcites are good and novel active materials for Zn–Ni secondary cells.

Acknowledgments

We thank the National Natural Science Foundation of China (No. 91023031), Science and Technology Project of Changsha City in 2012 (No. K1203014-11) and Production, Teaching and Research Integrated Project of Guangdong Province and Ministry of Education (No. 2010B090400341) for their financial support.

References

[1] J. Jindra, J. Power Sources 88 (2000) 202–205.
[2] Y.F. Yuan, J.P. Tu, H.M. Wu, C.Q. Zhang, S.F. Wang, X.B. Zhao, J. Power Sources 165 (2007) 905–910.
[3] S.-H. Lee, C.-W. Yi, K. Kim, J. Phys. Chem. C 115 (2011) 2572–2577.
[4] R. Wen, Z. Yang, X. Fan, Z. Tan, B. Yang, Electrochim. Acta 83 (2012) 376–382.
[5] X. Fan, Z. Yang, W. Long, Z. Zhao, B. Yang, Electrochim. Acta 92 (2013) 365–370.
[6] M. Geng, D.O. Northwood, Int. J. Hydrogen Energy 28 (2003) 633–636.
[7] Y.-D. Cho, G.T.-K. Fey, J. Power Sources 184 (2008) 610–616.
[8] Y.F. Yuan, J.P. Tu, H.M. Wu, B. Zhang, X.H. Huang, X.B. Zhao, Electrochem. Commun. 8 (2006) 653–657.
[9] D. Zeng, Z. Yang, S. Wang, X. Ni, D. Ai, Q. Zhang, Electrochim. Acta 56 (2009) 4075–4080.
[10] R. Shivkumar, G.P. Kalaignan, T. Vasudevan, J. Power Sources 75 (1998) 90–100.
[11] J. Zhu, Y. Zhou, C. Gao, J. Power Sources 72 (1998) 231–235.
[12] R. Renuka, S. Ramamurthy, K. Muralidharan, J. Power Sources 76 (1998) 197–209.
[13] J. Yu, H. Yang, X. Ai, X. Zhu, J. Power Sources 103 (2001) 93–97.
[14] S.R. Oliver, Chem. Soc. Rev. 38 (2009) 1868–1881.
[15] Poernomo Gunawan, Rong Xu, Chem. Mater. 21 (2009) 781–783.
[16] L. Du, B. Qu, J. Mater. Chem. 16 (2006) 1549–1554.
[17] F. Zhang, L. Zhao, H. Chen, S. Xu, D.G. Evans, X. Duan, Angew. Chem. Int. Ed. 47 (2008) 2466–2469.
[18] L. Guadagnini, A. Mignani, E. Scavetta, D. Tonelli, Electrochim. Acta 55 (2010) 1217–1220.
[19] B.R. Shaw, J. Electrochem. Soc. 137 (1990) 3136–3143.
[20] H. Chen, J.M. Wang, T. Pan, H.M. Xiao, J.Q. Zhang, C.N. Cao, Int. J. Hydrogen Energy 27 (2002) 489–496.
[21] R. Roto, A. Yamagishi, G. Villemure, J. Electroanal. Chem. 572 (2004) 101–108.
[22] X. Fan, Z. Yang, R. Wen, B. Yang, W. Long, J. Power Sources 224 (2013) 80–85.
[23] M.G. Perez, M.J. O'Keefe, T. O'Keefe, D. Ludlow, J. Appl. Electrochem. 37 (2006) 225–231.
[24] Z. Ji-ling, Z. Yun-hong, Y. Hanxi, J. Power Sources 69 (1997) 169–173.
[25] H. Yang, X. Meng, E. Yang, X. Wang, Z. Zhou, J. Electrochem. Soc. 151 (2004) A389–A393.
[26] D.G. Evans, X. Duan, Chem. Commun. (2006) 485–496.
[27] M. Ma, J.P. Tu, Y.F. Yuan, X.L. Wang, K.F. Li, F. Mao, Z.Y. Zeng, J. Power Sources 179 (2008) 395–400.
[28] F. Touhami, A. Aouniti, Y. Abed, B. Hammouti, S. Kertit, A. Ramdani, K. Elkacemi, Corros. Sci. 42 (2000) 929–940.
[29] D. Mohan, C.U. Pittman Jr., J. Hazard. Mater. 137 (2006) 762–811.
[30] Z. Luo, S. Sang, Q. Wu, S. Liu, J. Electrochem. Soc. 2 (2012) A21–A24.